PERGAMON

Acta mater. Vol. 47, No. 17, pp. 4275–4282, 1999

Printed in Great Britain
PII: S1359-6454(99)00308-0
1359-6454/99 $20.00 + 0.00

A MODEL FOR THE LONGITUDINAL PRIMARY CREEP OF A LONG-FIBER COMPOSITE

T. A. VENKATESH† and D. C. DUNAND‡

Department of Materials Science and Engineering, Massachusetts Institute of Technology, Cambridge, MA 02139, U.S.A.

(Received 12 March 1999; accepted 13 August 1999)

Abstract—The longitudinal primary creep of long-fiber composites is modeled by considering the transient stress states arising from load transfer from the weaker matrix phase to the stronger fiber phase as the composite transitions from the elastic state present immediately after loading to steady-state stage where both phases creep. The effect of primary creep of each of the phases on the primary creep of the composite is also taken into account. The model is evaluated for the NiAl–W system for which the primary creep of tungsten fibers is quite significant. The composite primary creep strain is predicted to be significant at high applied composite stresses and for high fiber volume fractions and primary creep time is found to be uniquely related to the composite steady-state creep rate. The model is verified with 1025°C compressive creep experiments in the NiAl–W composite system. Good agreement between model predictions and experiments is obtained when the observed composite steady-state creep behavior converges to the steady-state predicted for materials in which both phases experience creep deformation. © *1999 Acta Metallurgica Inc. Published by Elsevier Science Ltd. All rights reserved.*

Keywords: High temperature; Creep; Intermetallics; Fibers; Composites

1. INTRODUCTION

Unidirectional long-fiber composites with their promise of high specific strength, stiffness and creep resistance have been the subject of considerable research effort. Their ambient temperature elastic and elasto-plastic properties in the longitudinal and transverse directions are well understood [1]. The high temperature creep behavior of composites reinforced with elastic fibers has been accurately modeled as well [2]. Composites reinforced with creeping fibers have been investigated mostly for the particular case where the life of the composite is dominated by the secondary creep regime. Continuum level mechanical models that correlate the secondary creep of the individual constituents with that of the composite have been developed and validated with experiments for a variety of metal matrix composites [2]. Since the primary creep of monolithic homogeneous materials [3] and ceramic fibers can be significant [4–6], a more general solution that incorporates the primary creep of the individual constituents of the composite needs to be developed.

McDanels [7] postulated qualitatively that fiber composites might exhibit primary creep transients due to a combination of load-transfer effects and primary creep of the matrix and the fiber. Blank [8] analyzed the composite primary creep behavior for the particular case where the matrix and fiber creep rates follow liner stress dependence. Park and Holmes [9] reported finite element results for the creep of fiber reinforced ceramic composites for the case where the matrix creep rate displays power-law stress dependence, but the fiber creep rate decreases monotonically with time and exhibits a linear stress dependence. DeSilva [10] developed a model and compared it with the copper–tungsten system for the case where the tungsten fiber and the copper matrix creep rates exhibit non-linear stress dependence, as discussed in more detail later.

The objectives of the present investigation are to develop and experimentally validate a general mechanics model for the longitudinal primary creep behavior of long-fiber composites, taking into account the effects of load transfer and creep of both phases. First, a model for the creep of long-fiber composites is derived for the general case where both fiber and matrix undergo time-independent elastic deformation as well as time-dependent plastic deformation by primary and secondary creep. Second, the model is numerically evaluated using the NiAl–W system for the case where tungsten fibers exhibit significant primary creep while that of the NiAl matrix is negligible. Third, the model is compared to the model developed earlier by DeSilva [10]. Finally, the model predictions are compared to experimental results from creep tests

†To whom all correspondence should be addressed.
‡Present address: Department of Materials Science and Engineering, Northwestern University, Evanston, IL 60208, USA

on NiAl composites reinforced with low volume fractions of tungsten fibers.

2. MODEL

The instantaneous elastic/elasto-plastic response as well as long-term creep behavior of uni-directional continuous fiber reinforced systems loaded in uni-axial compression [Fig. 1(a)] is modeled using a simple one-dimensional, non-linear spring–dashpot model [Fig. 1(b)]. The model developed here for uni-axial compression is equally valid for uni-axial tension. The springs and the dashpots capture the elastic and creep responses of the constituent phases, respectively. In developing the model, the following assumptions are made:

1. The in-plane material behavior (i.e. in the y–z plane) is representative of the bulk behavior of the composite.
2. Perfect bonding exists between the fiber and the matrix without interfacial slippage so that strain compatibility is maintained at all times during deformation.
3. The constituents are stress-free prior to loading.
4. Fibers are perfectly straight and parallel to the applied stress direction. In compression, no bending moments are introduced into the system.
5. Fiber volume fraction is low enough that inter-fiber interactions are negligible, allowing the use of a unit cell with a single fiber.
6. End effects are negligible.
7. The elastic and plastic Poisson's ratios of both constituents are identical.
8. Upon loading, the instantaneous elastic solutions for fiber and matrix stresses are valid.

Upon applying a compressive stress to the composite, the matrix and fiber stresses, at all times, are governed by mechanical equilibrium:

$$\sigma_{\text{comp}} = v_{\text{f}}\sigma_{\text{f}} + v_{\text{m}}\sigma_{\text{m}} \tag{1}$$

where subscripts m and f represent matrix and fiber, respectively, and $v_{\text{m}} = 1 - v_{\text{f}}$.

For a constant stress creep experiment where the composite stress σ_{comp} remains invariant with time, equation (1) yields

$$\dot{\sigma}_{\text{m}} = -\left[\frac{v_{\text{f}}}{v_{\text{m}}}\right]\dot{\sigma}_{\text{f}} \tag{2}$$

where $\dot{\sigma} = \mathrm{d}\sigma/\mathrm{d}t$. The steady-state, or secondary, creep rates of the matrix and the fiber follow power-law behavior with stress exponents n:

$$[\dot{\epsilon}_i]_{\text{ss}} = K_i[\sigma_i]^{n_i} \tag{3}$$

where $[\dot{\epsilon}_i]_{\text{ss}}$ represents steady state, or secondary, strain rate, subscript i represents matrix or fiber, and K is a constant that accounts for microstructural effects and activation energies for creep deformation. The strain (ϵ) and strain rate ($\dot{\epsilon}$) compatibility between the matrix and fiber dictate:

$$\epsilon_i = \epsilon_{\text{comp}} \tag{4}$$

$$\dot{\epsilon}_i = \dot{\epsilon}_{\text{comp}}. \tag{5}$$

At any given time the total strain in the matrix and fiber consists of elastic and plastic components:

$$\epsilon_i = \epsilon_i^{\text{elastic}} + \epsilon_i^{\text{plastic}} \tag{6}$$

where the plastic component has contributions from the primary transient and secondary steady-state creep regimes. The elastic strain is given by Hooke's law:

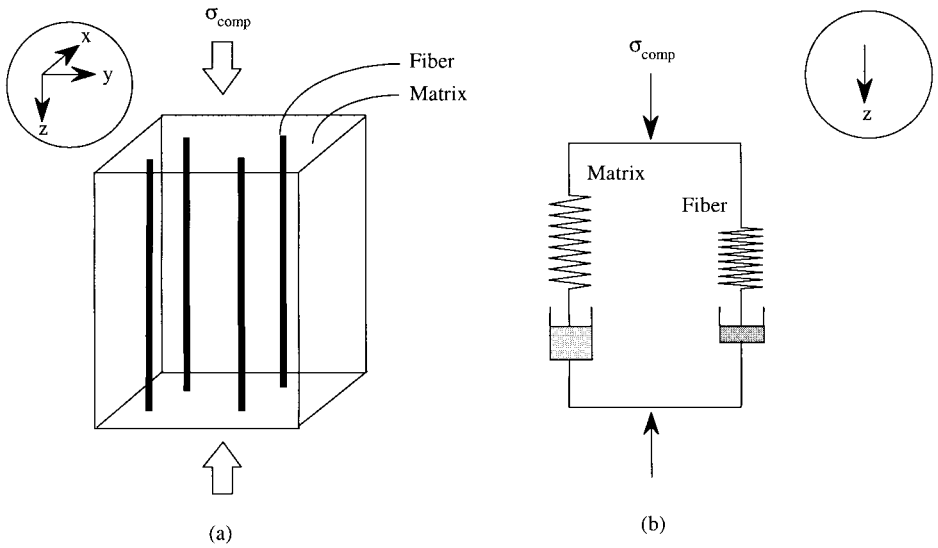

Fig. 1. Schematic of primary creep model.

$$\epsilon_i^{\text{elastic}} = \frac{\sigma_i}{E_i}. \quad (7)$$

The plastic strain can be modeled as

$$\epsilon_i^{\text{plastic}} \,|_{\sigma=\text{constant}} = [\dot{\epsilon}_i]_{\text{ss}} t + q_i t^{1/3} \quad (8)$$

where the primary creep transient is described with Andrade time law with an exponent of 1/3 [11] and q_{m}, for the purpose of illustration and without any loss in generality, is taken as a constant that exhibits a linear dependence with stress:

$$q_i = q_{0i} + q_{1i}\sigma_i \quad (9)$$

where the constants q_{0i} and q_{1i} can be determined from experiments.

From equations (8) and (9), the total plastic strain that accumulates under conditions of varying stresses is

$$\epsilon_i^{\text{plastic}} = \int_0^t \left(\left[\frac{1}{3}[q_{0i} + q_{1i}\sigma_i] t^{-2/3} \right] + [\dot{\epsilon}_i]_{\text{ss}} \right) \text{d}t. \quad (10)$$

Introducing equations (7) and (10) in the strain-compatibility condition of equation (4) leads to

$$\frac{\sigma_{\text{m}}}{E_{\text{m}}} + \int_0^t \left[\frac{1}{3}[q_{0\text{m}} + q_{1\text{m}}\sigma_{\text{m}}] t^{-2/3} + K_{\text{m}}[\sigma_{\text{m}}]^{n_{\text{m}}} \right] \text{d}t = \frac{\sigma_{\text{f}}}{E_{\text{f}}} + \int_0^t \left[\frac{1}{3}[q_{0\text{f}} + q_{1\text{f}}\sigma_{\text{f}}] t^{-2/3} + K_{\text{f}}[\sigma_{\text{f}}]^{n_{\text{f}}} \right] \text{d}t \quad (11)$$

where the left-hand side of the equation represents the total matrix strain, consisting of a first elastic term and a second plastic term, and the right-hand side is the total fiber strain.

Using equation (11) in the strain-rate compatibility condition, equation (5):

$$\frac{\dot{\sigma}_{\text{m}}}{E_{\text{m}}} + \frac{1}{3}([q_{0\text{m}} + q_{1\text{m}}\sigma_{\text{m}}] t^{-2/3}) + K_{\text{m}}[\sigma_{\text{m}}]^{n_{\text{m}}} = \frac{\dot{\sigma}_{\text{f}}}{E_{\text{f}}} + \frac{1}{3}([q_{0\text{f}} + q_{1\text{f}}\sigma_{\text{f}}] t^{-2/3}) + K_{\text{f}}[\sigma_{\text{f}}]^{n_{\text{f}}} \quad (12)$$

where the left-hand side of the equation represents the total matrix strain rate, consisting of a first elastic-rate term and a second plastic-rate term, and the right-hand side is the total fiber strain rate.

Introducing equations (1) and (2) in equation (12) and rearranging yields

$$\dot{\sigma}_{\text{f}} = \left\{ \frac{K_{\text{m}} \left[\frac{\sigma_{\text{comp}} - \sigma_{\text{f}} v_{\text{f}}}{v_{\text{m}}} \right]^{n_{\text{m}}} - K_{\text{f}} \sigma_{\text{f}}^{n_{\text{f}}} + \frac{1}{3} \left(q_{0\text{m}} + q_{1\text{m}} \left[\frac{\sigma_{\text{comp}} - \sigma_{\text{f}} v_{\text{f}}}{v_{\text{m}}} \right] - q_{0\text{f}} - q_{1\text{f}}\sigma_{\text{f}} \right) t^{-2/3}}{\frac{1}{E_{\text{f}}} + \left[\frac{v_{\text{f}}}{v_{\text{m}}} \right] \frac{1}{E_{\text{m}}}} \right\}. \quad (13)$$

In the most general case for any arbitrary value for n_{m} and n_{f}, this differential equation does not lend itself to an analytical solution. Hence it is solved numerically using the standard Runge–Kutta method for fiber stress as a function of time, subject to the initial condition that upon loading at time $t = 0$, the stress in the fiber is

$$\sigma_{\text{f}} \,|_{t=0} = \frac{\sigma_{\text{comp}}}{\left[v_{\text{f}} + v_{\text{m}} \frac{E_{\text{m}}}{E_{\text{f}}} \right]} \quad (14)$$

as dictated by the elastic solution, where equations (1), (4) and (7) were used.

The composite strain rates and strains are then computed as functions of time from equations (11) and (12). At very long times, the composite creep rate is expected to converge to the corresponding steady-state creep rate $\dot{\epsilon}_{\text{ss}}$ given by McLean [2] as

$$\sigma_{\text{comp}} = v_{\text{f}} \left[\frac{\dot{\epsilon}_{\text{ss}}}{K_{\text{f}}} \right]^{1/n_{\text{f}}} + [1 - v_{\text{f}}] \left[\frac{\dot{\epsilon}_{\text{ss}}}{K_{\text{m}}} \right]^{1/n_{\text{m}}}. \quad (15)$$

The steady-state fiber and matrix stresses are then given as

$$\sigma_i \,|_{\text{ss}} = \left[\frac{\dot{\epsilon}_{\text{ss}}}{K_i} \right]^{1/n_i}. \quad (16)$$

If the matrix primary is insignificant, i.e. $\epsilon_{\text{m}}^{\text{primary}} = 0$, equation (13) can be rewritten as

$$\dot{\sigma}_{\text{f}} = \left(\frac{K_{\text{m}} \left[\frac{\sigma_{\text{comp}} - \sigma_{\text{f}} v_{\text{f}}}{v_{\text{m}}} \right]^{n_{\text{m}}} - K_{\text{f}} \sigma_{\text{f}}^{n_{\text{f}}} + \frac{1}{3}[-q_{0\text{f}} - q_{1\text{f}}\sigma_{\text{f}}] t^{-2/3}}{\frac{1}{E_{\text{f}}} + \left[\frac{v_{\text{f}}}{v_{\text{m}}} \right] \frac{1}{E_{\text{m}}}} \right) \quad (17)$$

and solved numerically for composite strain rates and strains as indicated above.

DeSilva [10] models the primary creep of long-fiber composites (Appendix A) using the principle of virtual displacements assuming the stress relaxation in the matrix to be accommodated entirely by elastic strains [equation (A3)]. DeSilva's model can be compared to the model presented in this paper by using explicit expressions for the matrix and fiber strains:

$$\epsilon_{\text{m}}(\sigma_{\text{m}}, t) = \frac{\sigma_{\text{m}}}{E_{\text{m}}} + \int_0^t (K_{\text{m}}[\sigma_{\text{m}}]^{n_{\text{m}}}) \text{d}t \quad (18)$$

$$\epsilon_{\text{f}}(\sigma_{\text{f}}, t) = \frac{\sigma_{\text{f}}}{E_{\text{f}}} + \int_0^t \left[\frac{1}{3}[q_{0\text{f}} + q_{1\text{f}}\sigma_{\text{f}}] t^{-2/3} + K_{\text{f}}[\sigma_{\text{f}}]^{n_{\text{f}}} \right] \text{d}t. \quad (19)$$

Table 1. 1025°C input parameters for the primary creep model [12–14]. Measured stress range in parentheses

Property	NiAl	W
E (GPa)	128 GPa [15]	366 GPa [15]
K (/MPa^n s)	6.37×10^{-14} (15–32 MPa)	3.48×10^{-26} (450–720 MPa)
n	5.6	6.77
q_0 (/MPa)	0	-2.82×10^{-4}
q_1 (/MPa)	0	8.64×10^{-7}

Introducing equations (18) and (19) with only the plastic component of strain (i.e. with the terms σ_i/E_i set to zero), in equations (A6), (A7) and (A12), the rate of change in the matrix stress with time obtained from DeSilva's approach also transforms to equation (17) developed in this work. Thus, despite the different derivation paths taken in the two approaches, the expressions for the evolution of fiber and matrix stresses with time are the same, as the fundamental strain compatibility criterion between the deforming phases are satisfied in both approaches.

We could also model the case of weak interfaces that could allow for slip across the fiber–matrix interface, for which the strain-compatibility criterion may not necessarily hold. In this case the results from the two approaches would be different. However, we do not address such a case as our experimental results have been obtained from a system that exhibits strong interfaces.

3. APPLICATION OF THE MODEL TO NiAl–W COMPOSITES

The model developed in the previous section is applied to characterize the creep response of a NiAl–W composite under a compressive stress of 120 MPa at 1025°C where both phases are expected to creep. The various input parameters are given in Table 1 and were measured independently on NiAl and tungsten [13].

As shown in Fig. 2, upon loading a 15 vol.% tungsten composite to 120 MPa, the stresses in the fiber and matrix evolve from their elastic values of 268 and 94 MPa [equation (14)] to their respective steady-state values of 700 and 18 MPa [equation (16)] over a time-scale of 10,000 s. As there is a singularity in the stress solution at time $t=0$, the initial time used in numerical simulations is set at 0.001 s. The subsequent time-steps for the numerical computations are typically on the order of 1 s.

Over the same time-span, the contribution to total fiber strain rate from the elastic and plastic (i.e. primary and secondary) parts is illustrated in Fig. 3. At very short times ($t < 4$ s) the elastic strain rate term dominates, while at longer times ($t >$ 2000 s) it becomes vanishingly small. This is to be expected as the fiber stress changes rapidly at short times and remains virtually unchanged at longer times (Fig. 2). At short times, the primary part of the plastic rate dominates over the secondary part of the plastic rate while at longer times, the secondary term dominates and determines almost entirely the total fiber strain rate [equation (12)].

The composite creep strains can then be calculated as a function of time under three different conditions, as shown in Fig. 4.

a. Using McLean's model [equations (3) and (10) with $q_m=0$] assuming the composite reaches a steady-state instantaneously upon loading. In this case the creep curve is linear in time as the

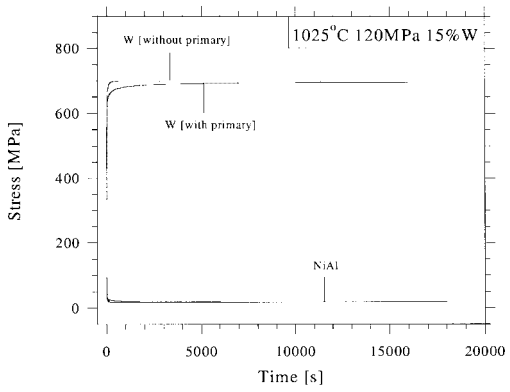

Fig. 2. Modeling the evolution of stresses in NiAl and tungsten from the primary to secondary stage for a NiAl–15 vol.% W composite at 1025°C and under a stress of 120 MPa.

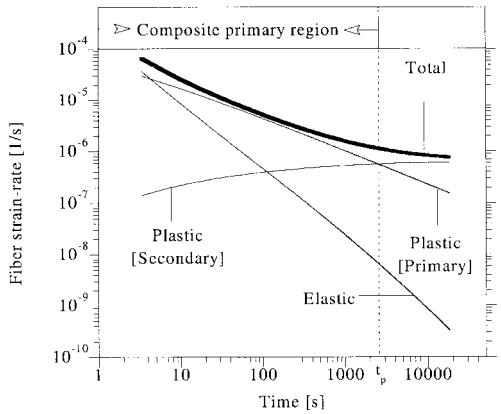

Fig. 3. Model predictions for the evolution of primary and secondary contributions to the fiber creep rate in a NiAl composite with 15 vol.% W at 120 MPa and 1025°C.

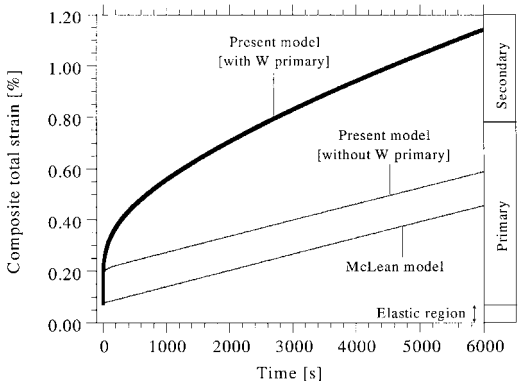

Fig. 4. Model predictions for the composite creep strain as a function of time with and without tungsten primary contribution (120 MPa, 15 vol.% W, 1025°C).

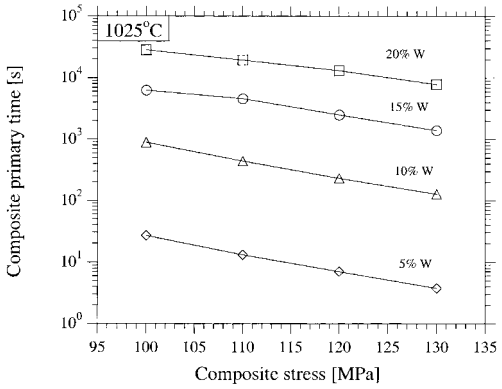

Fig. 6. Model predictions for the variation of composite primary time (with tungsten primary contribution) with applied composite stress.

composite creeps at a constant steady-state strain rate from $t=0$ [equation (15)].

b. Using the present model, but ignoring the primary creep regime in tungsten [equation (17) with $q_f=0$]. Then, the composite creep curve exhibits a primary region due solely to load transfer from matrix to fiber (Fig. 2), followed by a secondary region where the creep rate remains constant and equal to the steady-state strain rate [equation (15)].

c. Using the present model, but incorporating the primary creep regime in tungsten [equation (17)]. In this case, the composite exhibits a primary region that is more pronounced and extended over longer times compared to case (b) and followed by a secondary region. As expected, the composite creep strain predicted by this model is higher than for case (a) or (b) above.

This model (case c) is then applied to systematically investigate the primary creep behavior of NiAl–W composites at 1025°C for a range of stresses (100–130 MPa) and fiber volume fractions (5–20 vol.%).

The two most important parameters that characterize the composite primary regime are:

- Total primary-creep strain accumulated by the composite ϵ_p (Fig. 4) defined as the total strain that is accumulated by the composite while the plastic primary region is dominant.
- Total time over which the primary region is dominant t_p (Fig. 3) defined as the time over which the primary plastic-rate contribution is greater than the secondary plastic-rate contribution (Fig. 3).

The primary creep strain ϵ_p exhibits a complex dependence with changes in applied stress and reinforcement volume fraction at a given temperature (Fig. 5). This is because primary creep strains are integrated from strain-rate transients whose dependence on the composite stresses and volume fractions is complex.

The primary time t_p on the other hand, decreases with applied stress for the four volume fractions investigated (Fig. 6). As shown in Fig. 7, t_p can be uniquely related to the steady-state strain rate of the composite through the following empirical relation:

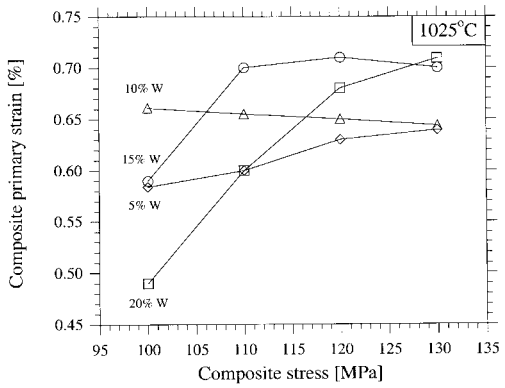

Fig. 5. Model predictions for the variation of composite primary creep strain (with tungsten primary contribution) with applied composite stress.

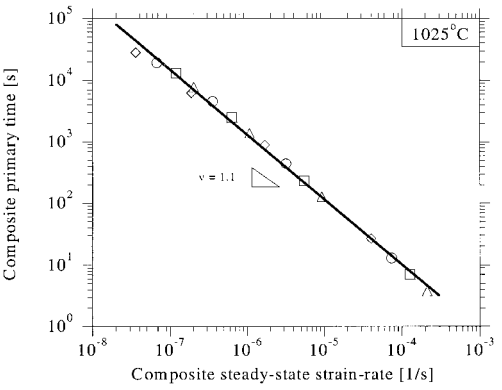

Fig. 7. Model predictions for the variation of composite primary time (with tungsten primary contribution) with the composite steady-state strain rate and empirical fit (same symbols as Fig. 6).

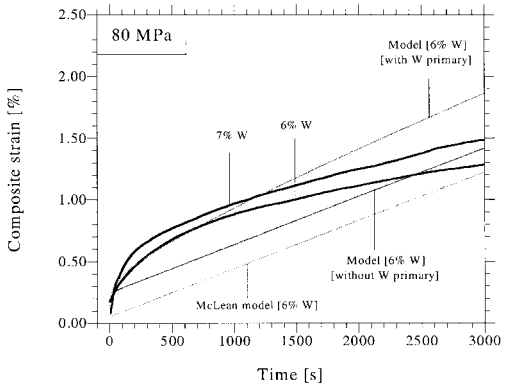

Fig. 8. Comparison of theoretically predicted with experimentally observed creep behavior of NiAl composites with 6 and 7 vol.% W (experiments 1 and 2, respectively, in Ref. [13]) at 80 MPa and 1025°C.

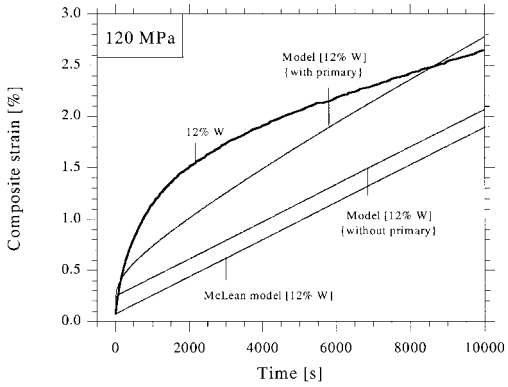

Fig. 10. Comparison of theoretically predicted with experimentally observed creep behavior for NiAl composites with 12 vol.% W (experiment 9 in Ref. [13]) at 120 MPa and 1025°C.

$$t_p[\dot{\epsilon}_{ss}]^{\nu} = \lambda \tag{20}$$

where the parameters ν and λ are 1.1 and 6×10^{-4}/ $s^{0.1}$, respectively, for the range of parameters studied here.

4. EXPERIMENTAL VERIFICATION OF MODEL

The primary and secondary creep behavior of NiAl and tungsten fibers were characterized at 1025°C, as reported in detail in Refs [12–14]. It was found that NiAl exhibited negligible primary creep while the primary creep of tungsten was significant and could be described by the Andrade time law [equations (8) and (9)] with an exponent of 1/3. Creep parameters of NiAl and tungsten are summarized in Table 1. Compression creep experiments were carried out on NiAl reinforced with 6–16 vol.% of tungsten fibers [12–14] at two different stress levels, 80 and 120 MPa. Figures 8–13 show the primary creep sections of a selection of creep curves reported in Ref. [13].

In most cases (Figs 8–13), experimentally obtained creep curves exhibit reasonable agreement with model predictions for the spectrum of volume fractions investigated. For cases where there exists a good correlation between the predicted and the observed steady-state creep rates, there is also a good correlation between the predicted and observed primary creep strains [12, 13]. As the strain-rate transients converge to the predicted steady-state creep rates the primary creep strains computed by integration of strain-rate transients are also expected to converge to the observed values.

Reasons for the observed discrepancy between experiments and model predictions are discussed as follows:

1. The NiAl–W composites were fabricated through the reactive infiltration process as described in detail in Ref. [13]. Due to the high temperatures involved in this processing technique, the tungsten fibers were partially recrystallized. As the tungsten creep results were obtained from exper-

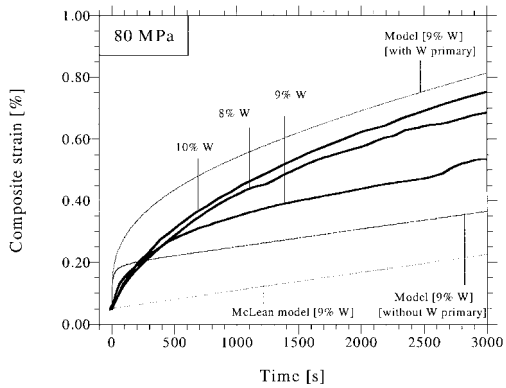

Fig. 9. Comparison of theoretically predicted with experimentally observed creep behavior of NiAl composites with 8, 9 and 10 vol.% W (experiments 4, 5 and 6, respectively, in Ref. [13]) at 80 MPa and 1025°C.

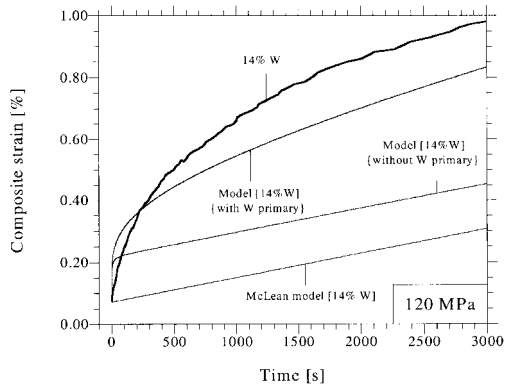

Fig. 11. Comparison of theoretically predicted with experimentally observed creep behavior of NiAl composites with 14 vol.% W (experiment 13 in Ref. [13]) at 120 MPa and 1025°C.

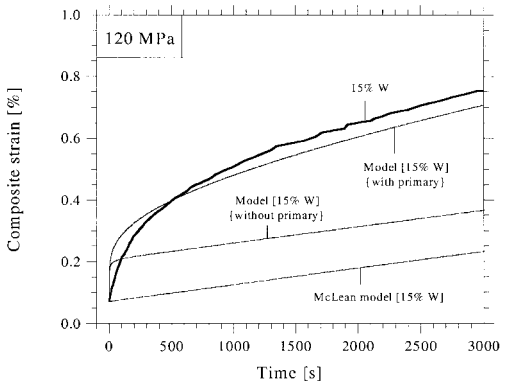

Fig. 12. Comparison of theoretically predicted with experimentally observed creep behavior of NiAl composites with 15 vol.% W (experiment 14 in Ref. [13]) at 120 MPa and 1025°C.

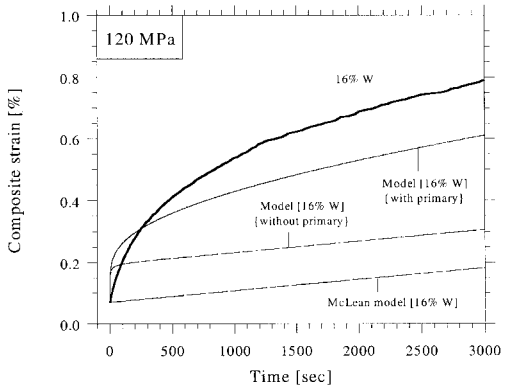

Fig. 13. Comparison of theoretically predicted with experimentally observed creep behavior of NiAl composites with 16 vol.% W (experiment 15 in REf. [13]) at 120 MPa and 1025°C.

iments on unrecrystallized tungsten, the effects of recrystallization have not been incorporated. Recrystallization is expected to influence both the primary and secondary creep behavior of tungsten, thus influencing the primary creep of the NiAl–W composites.

2. During reactive infiltration processing of NiAl–W composites, up to 2 at.% of tungsten from the tungsten fibers could dissolve in the NiAl matrix and subsequently reprecipitate at the NiAl grain boundaries. As NiAl creep results were obtained from reactive infiltration of nickel preforms that did not have any tungsten fibers, the effect of tungsten dissolution/reprecipitation on the secondary creep behavior of NiAl and thus the primary creep behavior of the NiAl–W composite has not been quantified.
3. In general the tungsten fibers were reasonably well aligned. However, as it was not possible to determine the alignment of the embedded fibers without destroying the samples, any misalignment of the tungsten embedded fibers in the tested samples could not be completely ruled out.

Thus the observed correlation between experiments and model predictions (which in most cases is within a factor of two) can be considered satisfactorily.

5. CONCLUSIONS

The longitudinal primary creep response of long-fiber composites was investigated for the general case where both the matrix and the fiber undergo plastic deformation by creep and exhibit primary and secondary creep regimes.

1. A methodology was developed that solved for the transient stress states while loads are transferred from the weaker phase (matrix) to the stronger phase (fiber) as the composite transitions from the elastic state present at loading to steady states attained at long times when both phases exhibit secondary creep.
2. This model was evaluated numerically for the NiAl–W system for the case where the primary creep of the NiAl matrix was negligible while that of tungsten fibers was quite significant. The model predicted:
   a. composite primary creep to be more significant at relatively high applied stresses and for composites with high volume fraction of reinforcements;
   b. primary creep strain to vary with stresses and reinforcement volume fraction in a complex manner; and
   c. primary creep time to be uniquely linked to the composite secondary creep rate.
3. Good agreement between the primary creep model predictions and experiments is obtained when the observed composite steady-state creep behavior converges to the predicted secondary composite steady state.

Acknowledgements—This work was supported by the National Science Foundation through grant MSS 9201843, monitored by B. McDonald. T.A.V. and D.C.D. acknowledge the financial support of the Department of Materials Science and Engineering at MIT in the form of teaching assistanships and the AMAX career development chair, respectively. T.A.V. also acknowledges S. Suresh for funding in the form of a post-doctoral position at MIT during which time the preparation of this manuscript was completed.

REFERENCES

1. Chawla, K. K., *Composite Materials*. Springer-Verlag, New York, 1987.
2. McLean, M., *Mechanical Behavior of In-Situ Composites*. The Metals Society, London, 1983.
3. Cadek, J., *Creep in Metallic Materials*. Elsevier, New York, 1988.

4. Lewinsohn, C. A., Giannuzzi, L. A., Bakis, C. E. and Tressler, R. E., *J. Am. Ceram. Soc.*, 1999, **82**, 407.
5. Jia, N., Bodet, R. and Tressler, R. E., *J. Am. Ceram. Soc.*, 1993, **76**, 3051.
6. Bodet, R., Lamon, J., Jia, N. and Tressler, R. E., *J. Am. Ceram. Soc.*, 1996, **79**, 2673.
7. McDanels, D., Signorelli, R. A. and Weeton, J. W., Report No. TN D-4173, NASA, (1967).
8. Blank, E., in *Mechanical and Physical Behavior of Metallic and Ceramic Composites*, ed. S. I. Andersen, H. Lilholt and O. B. Pedersen. Risø National Laboratory, Roskilde, Denmark, 1988, p. 303.
9. Park, Y. H. and Holmes, J. W., *J. Mater. Sci.*, 1992, **27**, 6341.
10. DeSilva, A. R. T., in *Advances in Composite Materials*, ed. A. R. Bunsell, C. Bathias, A. Martrenchar, D. Menkes and G. Verchery. Pergamon Press, New York, 1980, p. 1115.
11. Andrade, E. N. D. C., *Proc. R. Soc. Lond.*, 1910, **A84**, 1.
12. Venkatesh, T. A. Doctoral thesis, Massachusetts Institute of Technology, Cambridge, MA, (1998)
13. Venkatesh, T. A. and Dunand, D. C., *Metall. Trans.*, in press
14. Venkatesh, T. A. and Dunand, D. C., in *Deformation and Fracture of Ordered Intermetallic Materials III*, ed. W. O. Soboyejo, T. S. Srivatsan and H. L. Fraser. The Minerals, Metals, and Materials Society, Warrandale, PA, 1996, p. 361.
15. Wright, P. K., Senmeier, M. D. and Kupperman, D. S., in *Measurement, Modeling, and Effects on Thermo-Mechanical Behavior*, ed. E. V. Barrera and I. Dutta. The Minerals, Metals, and Materials Society, Warrandale, PA, 1993, p. 131.

APPENDIX A

The model developed by DeSilva [10] for the primary creep of long-fiber composites is given below using DeSilva's original notation. Let λ_t be the extension of the composite at any instant t. In the next small time interval δ_t the matrix creeps a distance $\delta\xi$ under the influence of stress σ_m present at the beginning of the time-step:

$$\delta\xi = h_0 \frac{d\epsilon_m}{dt}\delta t \tag{A1}$$

where h_0 is the initial length of the composite, $d\epsilon_m/dt$ is the creep rate of the matrix at the beginning of the time-step. The fiber creeps a distance $\delta\eta$ given by a similar expression:

$$\delta\eta = h_0 \frac{d\epsilon_f}{dt}\delta t. \tag{A2}$$

In order to maintain strain compatibility between the phases, the composite extends an intermediate amount $\delta\lambda_t$. Therefore, during the interval δt the matrix relaxes its stress by $(-\delta\sigma_m)$ given by

$$-\delta\sigma_m = E_m\left[\frac{\delta\xi - \delta\lambda_t}{h_0}\right]. \tag{A3}$$

As the total composite stress remains constant, the decrease in matrix stress is matched by a corresponding increase in the fiber stress weighted by corresponding volume fractions obeying rule of mixtures given as

$$E_m\left[\frac{\delta\xi - \delta\lambda_t}{h_0}\right]v_m = E_f\left[\frac{\delta\lambda_t - \delta\eta}{h_0}\right]v_f. \tag{A4}$$

From equations (A1)–(A4) the rate of change of matrix stress with time is given as

$$\frac{d\sigma_m}{dt} = \frac{\left[\frac{d\epsilon_f}{dt} - \frac{d\epsilon_m}{dt}\right]}{\left[\frac{1}{E_m} + \frac{v_m}{v_f E_f}\right]}. \tag{A5}$$

Matrix and fiber strains are modeled as functions of stress and time as

$$\epsilon_m = \psi_m(\sigma_m, t) \tag{A6}$$

$$\epsilon_f = \psi_f(\sigma_f, t) \tag{A7}$$

and matrix and fiber strain rates are given as

$$\frac{d\epsilon_m}{dt} = \frac{\partial\psi_m}{\partial\sigma_m}\frac{d\sigma_m}{dt} + \frac{\partial\psi_m}{\partial t} \tag{A8}$$

and

$$\frac{d\epsilon_f}{dt} = \frac{\partial\psi_f}{\partial\sigma_f}\frac{d\sigma_f}{dt} + \frac{\partial\psi_f}{\partial t}. \tag{A9}$$

Under constant stress conditions, the fiber and matrix stress changes are related as

$$\dot{\sigma}_m = -\left[\frac{v_f}{v_m}\right]\dot{\sigma}_f. \tag{A10}$$

Substituting equation (A10) in equation (A9):

$$\frac{d\epsilon_f}{dt} = -\frac{v_m}{v_f}\frac{\partial\psi_f}{\partial\sigma_f}\frac{d\sigma_m}{dt} + \frac{\partial\psi_f}{\partial t}. \tag{A11}$$

Using equations (A5) and (A11), the rate of change of matrix stress with time is then given as

$$-\frac{d\sigma_m}{dt} = \frac{\left[\frac{\delta\psi_m}{\delta t} - \frac{\delta\psi_f}{\delta t}\right]}{\left[\frac{1}{E_m} + \frac{v_m}{v_f E_f} + \frac{\delta\psi_m}{\delta\sigma_m} + \frac{v_m}{v_f}\frac{\delta\psi_f}{\delta\sigma_f}\right]}. \tag{A12}$$